Journal of Catalysis **186,** 279–295 (1999)
Article ID jcat.1999.2563, available online at http://www.idealibrary.com on IDEAL®

A Study of the Reactions of Ethanol on CeO_2 and Pd/CeO_2 by Steady State Reactions, Temperature Programmed Desorption, and *In Situ* FT-IR

A. Yee, S. J. Morrison, and H. Idriss

Materials Chemistry, Department of Chemistry, The University of Auckland, Private Bag 92019, Auckland, New Zealand

Received December 23, 1998; revised March 31, 1999; accepted April 29, 1999

The reaction of ethanol on unreduced and H_2-reduced CeO_2 and 1 wt% Pd/CeO_2 has been investigated by steady state reactions, temperature programmed desorption (TPD), and *in situ* Fourier transform infrared (FT-IR) spectroscopy. Steady state reactions have shown a zero reaction order dependency for diatomic oxygen at and above 20%, whilst the addition of Pd to CeO_2 decreases the apparent activation energy of the reaction from 75 kJ mol^{-1} on CeO_2 alone to 40 kJ mol^{-1} (Pd/CeO_2). TPD experiments following ethanol adsorption on both CeO_2 and Pd/CeO_2 have shown desorption profiles corresponding to unreacted ethanol and various reaction and decomposition products (acetaldehyde, acetone, CO, CO_2, and methane). Ethanol conversion to reaction products was increased by the addition of Pd, from 15 and 30% on CeO_2 and H_2-reduced CeO_2, to 71 and 63% on Pd/CeO_2 and H_2-reduced Pd/CeO_2, respectively. Acetaldehyde desorbed in two temperature domains on CeO_2, and desorbed as one peak only on H_2-reduced CeO_2 (555 K), Pd/CeO_2 (395 K), and H_2-reduced Pd/CeO_2 (410 K). Desorption of acetone was observed on all surfaces; however, the desorption temperatures were considerably lower on Pd/CeO_2 than on CeO_2, suggesting that the formation of acetone on Pd/CeO_2 occurs from a different reaction pathway from that of CeO_2. Benzene formation was detected only on Pd/CeO_2 catalysts, with the H_2-reduced Pd/CeO_2 catalyst decreasing benzene formation to almost negligible amounts. FT-IR results have shown that ethanol adsorbs dissociatively at room temperature to form adsorbed ethoxide species on all surfaces studied. Acetate species (ν_{as}(OCO) 1572 cm^{-1} and ν_s(OCO) 1424 cm^{-1}) were detected on the unreduced CeO_2 surface at room temperature. In contrast, H_2-reduced CeO_2, as well as "as prepared" Pd/CeO_2, did not show evidence of acetates at room temperature. The decrease of the XPS O(1*s*)/Ce(3*d*) ratio in the case of Pd/CeO_2 (1.76) together with the absence of acetate formation may indicate partial reduction of the CeO_2 support upon the addition of Pd. Adsorbed acetaldehyde was detected on Pd/CeO_2 (1711 cm^{-1}) and H_2-reduced Pd/CeO_2 (1704 cm^{-1}) upon heating to 373 and 423 K, respectively. Adsorbed crotonaldehyde (ν(CO) ca. 1651 and ν(C=C) ca. 1634 cm^{-1}), from the β-aldolisation of two acetaldehyde molecules, was observed on both unreduced and high temperature reduced Pd/CeO_2 at 473 K. Carbonates were the remaining species at 625 K and above.

INTRODUCTION

The use of oxygenated hydrocarbons as fuels and fuel additives, together with the development of improved catalytic converters, is instrumental in meeting the high standards imposed on exhaust emission levels from vehicles. Three-way catalytic converters have made a significant contribution to reducing emission levels, by simultaneously converting hydrocarbons, carbon monoxide, and nitrogen oxides into nontoxic products. Three-way catalyst (TWC) compositions usually include up to 30 wt% of CeO_2 in the Al_2O_3 washcoat. Apart from its role as an oxygen storage component (1, 2), CeO_2 is also associated with thermal stabilisation of the alumina support (3), promotion of water–gas shift activity (4), promotion of Au/MnO_x catalysts for CO oxidation (5), and dispersion of the active noble metal phase (6, 7).

CeO_2 possesses the face centred cubic fluorite structure, which consists of a cubic close packed array of Ce^{4+} cations with all tetrahedral holes occupied by oxygen. In reductive atmospheres, Ce^{4+} ions on a stoichiometric surface are readily reduced to Ce^{3+}. This enables the reversible addition and removal of oxygen, thus allowing CeO_2 to act as an oxygen storage material in oxidation reactions. The Ce^{4+} to Ce^{3+} reduction is accompanied by the formation of oxygen vacancies leading to the formation of a Ce_2O_3 phase at high temperatures. Hydrogen reduction of CeO_2 has been reported to begin at 473 K and to be a surface process, with reduction temperatures above 923 K required for bulk reduction (8). Hydrogen chemisorption on CeO_2 is dependent on its BET surface area and believed to be a pure surface process (9, 10). The interaction between hydrogen and CeO_2 at 195–500 K has been postulated to lead to a bronze-like $CeO_2H_{0.17}$ compound (11).

Oxygenates, such as methanol, ethanol, and methyl tertiary butyl ether, have been extensively used as fuels and fuel additives to enhance the burning efficiency of automotive fuels. In particular, alcohols have proven to be effective in the near complete elimination of emissions of

0021-9517/99 $30.00

benzene, olefins, complex hydrocarbons, and SO_2. Moreover, methanol and ethanol are now seriously considered as a source for fuel cell powered vehicles (12). However, the partial oxidation of alcohols produces aldehydes, such as formaldehyde and acetaldehyde, which pose a greater threat as carcinogens. A better understanding of the reaction pathways along which the desired conversions occur on current commercial catalyst systems is necessary in order to develop more suitable catalyst materials.

The main body of literature on alcohol reactions over CeO_2 containing catalysts concerns methanol oxidation (13–16). It has been widely observed that the reaction of alcohols on various surfaces results in the dissociation of the O–H bond to produce alkoxides as the primary step. Spectroscopic studies by various authors have identified three methoxide species (monodentate, bidentate, tridentate) from the adsorption of methanol on CeO_2 (16).

Generally, alcohols on oxide surfaces may undergo molecular adsorption through the oxygen lone pair followed by deprotonation to form alkoxides. On some surfaces dehydrogenation occurs to form aldehydes from primary alcohols and ketones from secondary alcohols (17). The oxidation of aldehydes may result in the formation of carboxylate species if the surface contains oxygen of sufficient mobility. Formate species from the adsorption of methanol on CeO_2 (13), ZnO (18), and $ZnAl_2O_4$ (19) have been reported; in contrast, no evidence of formate species has been identified on SiO_2 (20) or TiO_2 (21). The stability of the carboxylate species also depends on the nature of the material (22). Whilst acetate species decompose to CO_2 and CH_4 on ZnO (18) at approximately 750 K and to CO, CO_2, and CH_4 on CeO_2 (23) at ca. 700 K, acetate species on the surface of metals occur at much lower temperatures. For example, on Pd(111)-(2×2)O (24) acetates, formed from the adsorption of acetic acid, decompose at 305 K.

In addition to oxidation to acetates, other reaction pathways have been observed on oxide surfaces from C_2 oxygenates.

(1) Carbon–carbon bond formation from aldehydes is possible through aldolisation reactions. In particular, the β-aldolisation of two acetaldehyde molecules, with subsequent dehydration, produces crotonaldehyde. Such a reaction on a surface would require Lewis acid and base sites to bind the two molecules and abstract an α-hydrogen. Crotonaldehyde formation has been observed on the surfaces of CeO_2 (23), TiO_2 (25), Al_2O_3 (26), and β-UO_3 (26), among other surfaces, upon the adsorption of acetaldehyde.

(2) Abstraction of a hydrogen atom from acetaldehyde can yield an acetyl species, $CH_3C{=}O$. Acetyl species have previously been observed from ethanol on Pd(111) (27) and from acetaldehyde on Pd(110) (28), Pd/CeO_2 (23), and Pt-Na/SiO_2 (29). Further reaction of an acetyl with an adsorbed methyl group can result in the production of acetone (23). In effect, the formation of ketones can be achieved from two different pathways. The first, as described above, is from the reaction of an adsorbed acyl group with an alkyl group. The second pathway, first involving oxidation of aldehydes to carboxylates on the oxide surface, is achieved via coupling of two carboxylates to yield one molecule of ketone and one molecule of CO_2. This latter reaction has been observed on TiO_2 (25) from acetic acid and on CeO_2 (23), Cu/ZnO/Al_2O_3 (30), and β-UO_3 (26) from acetaldehyde.

In studies done by McCabe and Mitchell (31), two types of catalyst behaviour were observed for reactions of ethanol in feedstreams containing excess oxygen. The two types of catalyst were characterised by their propensity towards either oxidation of ethanol to acetaldehyde and CO_2 or dehydration to diethyl ether and ethylene. Catalysts (hopcalite, 0.1% Pt/Al_2O_3, MgO, 4% Mn/Al_2O_3) favouring ethanol oxidation possessed a strong base character, whilst those (10% W/Al_2O_3, ZrO_2, Al_2O_3) promoting dehydration had strong acidic properties. The reducibility and basicity of CeO_2 favour oxidation and aldolisation reactions (23), and it has been found to be a very effective promoter and support in metal catalysts for both hydrogenation and oxidation processes. In addition, reduced CeO_2 has been observed to be active for the reductive coupling of acetaldehyde to butene and butadiene (23), as well as cross-reductive coupling between acetaldehyde and benzaldehyde to form $C_6H_5CH{=}CHCH_3$ (32).

In the present work, temperature programmed desorption (TPD), steady state reactions and *in situ* Fourier transform infrared (FT-IR) spectroscopy have been employed to identify the reaction intermediates and products and provide kinetic data from the reactions of ethanol on reduced and unreduced CeO_2 and Pd/CeO_2. The aim of conducting such an investigation is gaining a fundamental understanding of the interactions between the metal oxide and oxygenate to aid in the elucidation of the mechanisms of reaction.

EXPERIMENTAL

1. *Catalyst Preparation*

Cerium oxide was prepared by precipitating a solution of cerium nitrate at pH 9 with ammonia; the resulting gel-like hydroxide precipitate was filtrated and washed. Upon drying at 373 K, it was calcined at 723 K for 5 h. The 1 wt% Pd/CeO_2 was prepared by impregnating the CeO_2 support with $PdCl_2$ in 1 M HCl. Specific surface area measurements were determined by physisorption of nitrogen at 77 K using a Quantasorb Jr. dynamic system. The specific surface areas of CeO_2 and 1 wt% Pd/CeO_2 were determined by the multipoint BET method and found to be 57 and 55 $m^2\ g^{-1}$, respectively.

2. X-Ray Photoelectron Spectroscopy (XPS)

XPS analysis was performed using a Kratos XSAM-800 model with an operating base pressure of ca. 10^{-9} Torr. Mg $K\alpha$($h\nu = 1253.6$ eV) radiation was used at 170 W. Collection of spectra was performed at a pass energy of 65 eV. Sample charging of up to 5 eV occurred under X-ray radiation. Binding energies were calibrated with respect to the signal of adventitious carbon (284.7 eV). The following binding energies were observed: XPS Ce ($3d_{5/2}$), 882.0 eV (consistent with CeO_2 (33)); XPS Pd($3d_{5/2}$), 336.5 eV (consistent with PdO (34)).

3. Steady State Reactions

Kinetic analysis was conducted with a fixed-bed reactor fitted in a programmable oven, with an operating range of up to 673 K and linked to a gas chromatograph (GC) via a six-way valve (containing a 1-mL loop). Ethanol, in a saturator at 273 K, was introduced via either a continuous flow of dry air, a mixture of dry air and helium, or helium only, depending on the experimental conditions. The GC was equipped with a flame ionisation detector (FID) and coupled to a PC running PEAKSIMPLE III software for data acquisition. A chromosorb 102 column ($L = 2$ m, $d = 0.318$ cm), with nitrogen as the carrier gas, was used for separation of organic compounds at 373 K. The gas, containing ethanol, was allowed to flow over the catalyst for 10 min at room temperature before samples were injected into the GC via the six-way valve. Several runs were done in order to obtain a consistent result for ethanol peak area. Several runs were then performed with varying flow rates and reaction temperatures. For Arrhenius plots, ethanol conversion was kept at $\leq$10%. Below ca. 450 K ethanol and acetaldehyde were the only observed products. Above 500 K, ethylene, acetone, and traces of ethyl acetate were observed.

4. Temperature Programmed Desorption (TPD)

TPD was performed using a fixed-bed reactor interfaced to a high vacuum chamber (HVC) equipped with a HIDEN quadrupole mass spectrometer (base pressure at ca. 5×10^{-8} Torr). The mass spectrometer was coupled to an IBM PC with software (MASSoft) that was capable of monitoring up to 500 masses simultaneously at a cycling rate of 1 min. For the TPD analysis performed in this work, masses 2 to 100 were scanned, with a cycling rate of 20 s. Temperature profiles were programmed by a temperature controller connected to a thermocouple placed inside the furnace in contact with the reactor bed.

Prior to reaction, the catalyst was heated for 2 h under air at 773 K before being allowed to cool to room temperature (under flowing air), except in the case of catalysts which were reduced under flowing hydrogen overnight. The reduced catalysts were allowed to cool under hydrogen. Once at room temperature, the gas flow was switched to helium (ultrapure) to remove the oxidising (or reducing) gas from the system. Typically, this took 1 h. Diverting the helium flow through a saturator containing ethanol for 15 min ensured coverage of the catalyst surface. The catalyst was then purged with helium to remove any weakly adsorbed ethanol from the surface, as well as to clean the reactor and lines. Typically, this took 1.5 h. The gas flow was introduced to the vacuum chamber via a pressure interface which consisted of a leak valve differentially pumped at ca. 10^{-1} Torr during operation, in order to drop the pressure before introduction into the high vacuum chamber. A constant operating pressure of 5×10^{-6} Torr was maintained in the HVC during all TPD runs. During the final 30 min of purging the gas flow was allowed to enter the HVC and the $m/e = 31$ signal (the dominant fragment of ethanol) was monitored until no further change in the signal was observed; then TPD reaction was commenced.

Relative yields of all the desorption products were determined following the work of Ko *et al.* (35) and other workers (36) which consisted of: (i) separation of the desorption peaks into different domains of temperature, (ii) analysis of the fragmentation pattern of each product separately, and then (iii) starting from the most intense fragment for each product (i.e., $m/e = 31$ for ethanol) and subtracting the corresponding amounts of its fragmentation pattern until the majority of the signals were accounted for. Yields of each species are reported as a fraction of the entire sum of products,

$$Y_i = \frac{PA_i \times CF_i \times Cn_i}{\sum_j^n PA_j \times CF_i \times Cn_j},$$

where

PA_i is the area under the peak,
CF_i is the correction factor,
Cn_j is the number of carbon atoms in the molecule, and
$j = i, \ldots, n$.

5. Infrared Spectroscopy

IR spectra were recorded using a Digilab FTS-60 Fourier transform spectrometer at a resolution of 4 cm^{-1} and 100 scans per spectrum. The catalyst sample was pressed into a self-supporting disc, ca. 15 mm in diameter, mounted into a sample holder and placed into a stainless steel *in situ* IR cell, equipped with CaF_2 windows and capable of operating at temperatures between 77 and 773 K. The cell was connected to a conventional glass vacuum line maintained at a base pressure of 6×10^{-5} Torr with a diffusion pump.

Because of its basic nature, CeO_2 binds carbonates readily; thus in order to obtain a clean surface, pretreatment temperatures greater than 1000 K are often required. In this study, a temperature of 755 K was found to be sufficient. This pretreatment consisted of heating the sample at

755 K under oxygen (1.50 Torr) for 30 min; upon evacuation this procedure was repeated once more.

Reduction of the catalysts was achieved either by heating under H_2 in batch conditions or by H_2 flow. CeO_2 was reduced at 765 K with H_2 flow for 17 h and cooled to room temperature (under H_2 flow). Pd/CeO_2 was reduced at 550 K (or 755 K for high temperature reduction) under H_2 (1.50 Torr) for 30 min; upon evacuation, H_2 (1.50 Torr) was readmitted to the cell at 550 K (755 K) for a further 30 min. A typical IR adsorption experiment involved dosing ethanol (1.50 Torr), degassed by several freeze–pump–thaw cycles, onto the sample at room temperature for 3 min. A spectrum was taken upon evacuating the cell for ca. 15 to 25 min. The cell was then sequentially heated and spectra were collected from 373 to 673 K in 50 K intervals. The spectra presented in this paper are obtained by subtracting the spectrum of the catalyst sample prior to adsorption from that of the adsorbed sample.

RESULTS

1. *Catalyst Characterisation*

Table 1 presents BET and XPS data of CeO_2 and Pd/CeO_2 catalysts. Both materials have very similar surface areas; however, addition of Pd resulted in a decrease the O to Ce ratio, indicating that partial reduction of the oxide support is occurring. Moreover, the Pd/Ce ratio at the surface and near surface is lower than the expected theoretical value by about 40%.

2. *Steady State Reaction*

Figure 1 shows the effect of changing the flow rate on ethanol conversion over CeO_2 in the presence (a) and absence (b) of oxygen at 424 K, as illustrated by the equation

$$\ln\left(\frac{1}{1-x}\right) = k\frac{w}{F},$$

where x is the degree of ethanol conversion $((C_{in}-C_{out})/C_{in})$, w is the catalyst weight (110 mg), and F the flow rate (mL min^{-1}). In both cases a linear relationship is observed between the degree of ethanol conversion and the contact time, indicating a first-order reaction with respect to ethanol. The slope of each line denotes the rate constant, k, which was found to be 0.27 and 0.07 mL g^{-1} s^{-1} in the presence and absence of oxygen, respectively.

TABLE 1

Surface Areas and Atomic Ratios of O/Ce and Pd/Ce from XPS of CeO_2 and 1 wt% Pd/CeO_2 (Expected Values in Brackets)

Catalyst	BET (m^2 g^{-1})	XPS	
		O(1s)/Ce($3d_{5/2,3/2}$)	Pd($3d_{5/2,3/2}$)/Ce($3d_{5/2,3/2}$)
CeO_2	57	2.44	—
1 wt% Pd/CeO_2	55	1.76	0.008 (0.016)

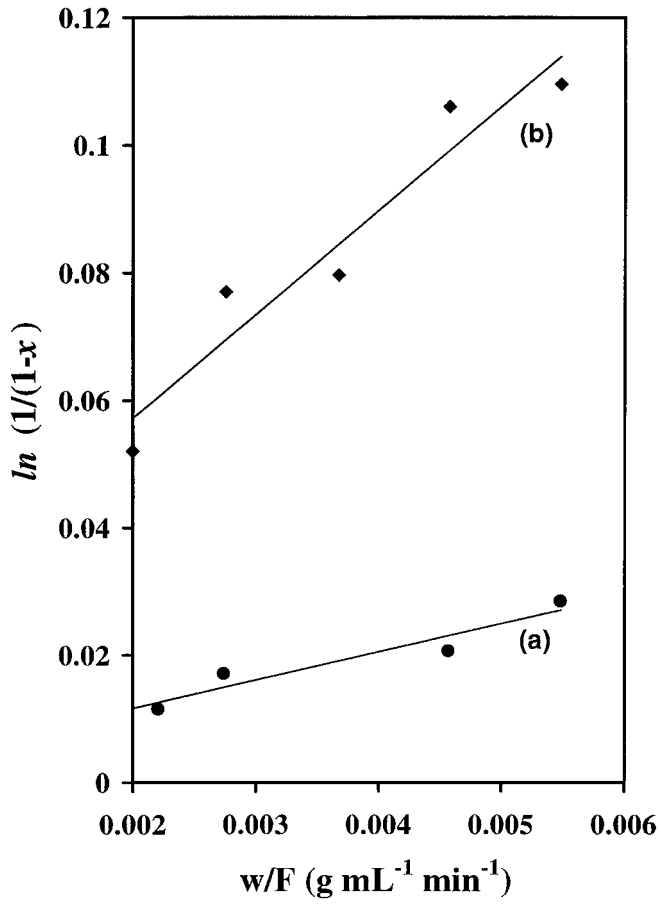

FIG. 1. Test of occurrence of first order kinetics for ethanol reaction over CeO_2 in gas concentrations: (a) 1.5% : 21% : 77.5% (ethanol : O_2 : N_2) and (b) 1.5% : 98.5% (ethanol : N_2). $T = 425$ K, $P = 1$ atm.

In order to investigate the role of gas-phase oxygen molecules, the reaction was performed with increasing amounts of inert gas displacing the oxygen, while keeping the ethanol concentration constant. The ratios of oxygen to inert gas were 14.2 : 1, 9.4 : 1, 4.7 : 1, and 0 : 1. Figure 2 shows the different kinetic parameters for ethanol reactions on CeO_2 as a function of oxygen concentrations at a constant flow rate of 1 mL s^{-1}. Thus, from the above results one can write the rate of reaction for ethanol over CeO_2 as

$$r = k[\text{ethanol}]^1 \cdot [O_2]^n$$

where n tends to zero at and above 20%. The reaction of ethanol with ethanol : O_2 : inert on CeO_2, passing over the catalyst at a constant flowrate of 1 mL s^{-1}, was tracked over a range of temperatures. For all runs, ethanol conversion was kept below 10% to assure operation in differential reactor conditions. Knowing that

$$k = A\exp\left(\frac{-E_A}{RT}\right),$$

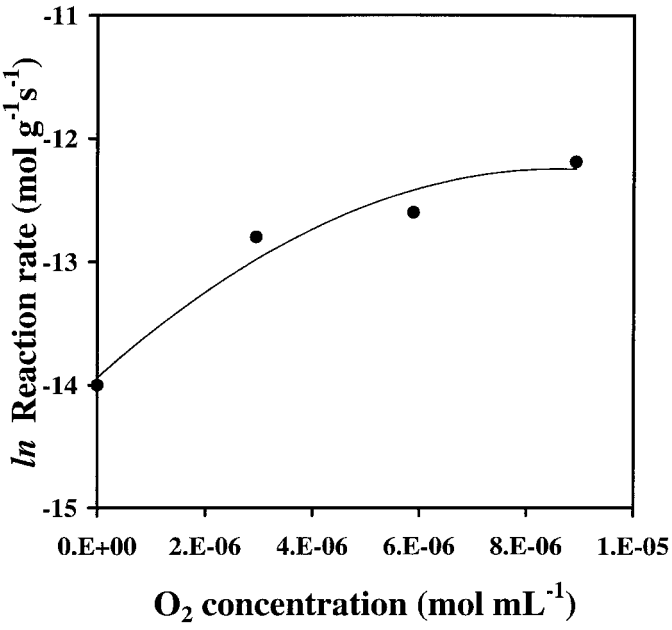

FIG. 2. Relationship between ln(reaction rate, r) and concentration of gas-phase O_2 for ethanol reaction over CeO_2. $T = 425$ K, $P = 1$ atm.

where k is the rate constant (mL g^{-1} s^{-1}), A the pre-exponential factor (mL g^{-1} s^{-1}), E_A the activation energy (J mol^{-1}), R the gas constant (J K^{-1} mol^{-1}), and T the reaction temperature (K), the apparent activation energy of the reaction, E_A, and the pre-exponential factor, A, can be computed (Table 2). In the presence of O_2, E_A is 75.4 kJ mol^{-1}. This value is lower than that of alcohol dehydrogenation reactions on MoO_3 (129 kJ mol^{-1}) (37), comparable to 1% Cr-CuO (76.9 kJ mol^{-1}) (38) and CuO (50.6 kJ mol^{-1}) (39), and higher than 1% Mn-CuO (33.5 kJ mol^{-1}) (38). Table 2 shows the kinetic data for CeO_2, Pd/CeO_2, and other catalysts. The addition of Pd decreased the activation energy by 35.5 kJ mol^{-1}. The pre-exponential factor has also decreased. However, the rate constant at relatively low temperatures is still much higher for Pd/CeO_2 than for CeO_2

TABLE 2

Summary of Kinetic Data for Ethanol on CeO_2, Unreduced 1 wt% Pd/CeO_2, and Various Catalysts (*a*) in the Presence of Oxygen (*b*) In the Absence of Oxygen: [Ethanol], 6.38×10^6 mol mL^{-1}; Flow, 60 mL min^{-1}; Weight, 110 mg; Reactor Volume, 13 mL

Catalyst	E_A (kJ mol^{-1})	A (mL g^{-1} s^{-1})	TON (400 K)	Ref.
$CeO_2^{(a)}$	75.4	3.81×10^9		This work
$CeO_2^{(b)}$	33	889		This work
MoO_3	129	—	—	(37)
CuO	50.6	3.1×10^5	—	(39)
1 wt% Cr/CuO	76.9	—	—	(38)
1 wt% Mn/CuO	33.5	—	—	(38)
1 wt% Pd/CeO_2	40.0	4.70×10^5	8.6	This work

TABLE 3

Product Analysis of Ethanol-TPD on Unreduced CeO_2

Product	Peak temperature (K)	Yield	Carbon selectivity (%)
Acetone	630	0.002	1.3
Acetaldehyde	455, 585	0.053, 0.042	34, 27
Carbon dioxide	690	0.015	9.7
Carbon monoxide	690	0.022	14
Ethanol	455, 585	0.508, 0.337	—
Methane	585	0.018	12

alone: $k_{393\,K} = 2$ and 0.3 mL g^{-1} s^{-1} for Pd/CeO_2 and CeO_2, respectively. The TON in Table 2 is calculated from the Pd XPS atomic concentration and BET data, assuming that 1 cm^2 contains 10^{15} atoms.

3. *Temperature Programmed Desorption (TPD)*

TPD after ethanol adsorption on unreduced CeO_2. Carbon yields of products desorbing during ethanol-TPD on unreduced CeO_2 surfaces are presented, along with carbon selectivity, in Table 3. Figure 3 shows the desorption

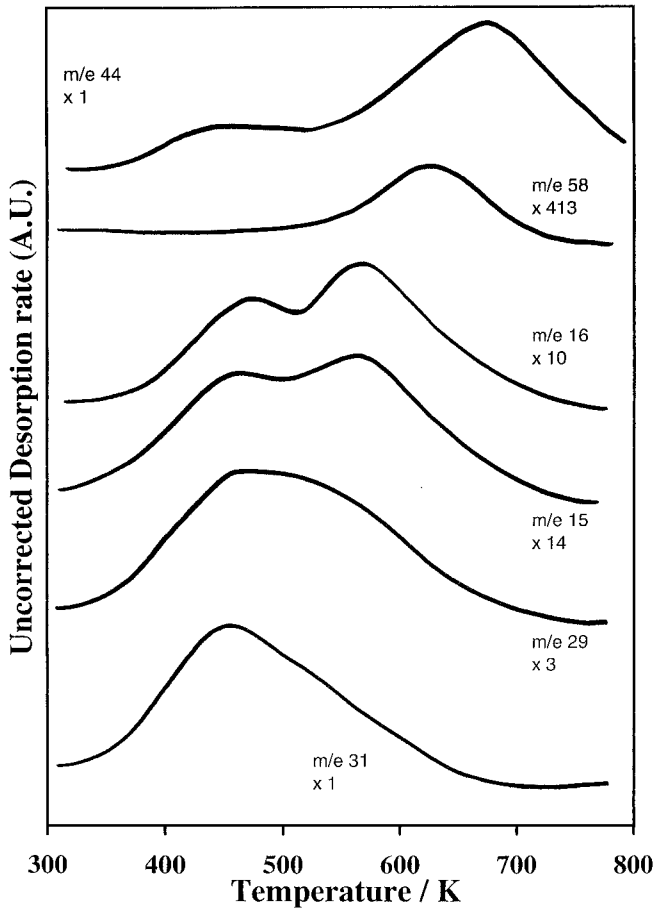

FIG. 3. Product desorption profiles from TPD after ethanol adsorption on unreduced CeO_2 at room temperature.

profiles of selected ion masses for ethanol-TPD on unreduced CeO_2 at a heating rate, β, of 10 K min^{-1}. There are four main temperature domains where desorption occurred. Acetaldehyde (CH_3CHO, $m/e = 29, 44, 43$), the major organic product, desorbed in two main temperature domains, at 455 and 585 K. The first desorption was the highest yielding, accounting for 5.3% of the total products. The twin desorption behaviour was mirrored with unreacted ethanol (CH_3CH_2OH, $m/e = 31, 45, 29$) which also desorbed at the same two temperatures as acetaldehyde. Unreacted ethanol was by far the largest desorption species, making up nearly 85% of the total carbon yield. A small amount of acetone (CH_3COCH_3, $m/e = 43, 58, 15$) was observed, desorbing at the second highest temperature domain of 630 K. Methane ($m/e = 16, 15, 14$) desorbed at 585 K, with carbon monoxide ($m/e = 28, 14$) and carbon dioxide ($m/e = 44, 28$) both desorbing at 690 K.

TPD after ethanol adsorption on H_2-reduced CeO_2. Product yields and selectivities for the H_2-reduced CeO_2 (H_2 reduction was performed at 1 atm., 773 K, for 12 h) are presented in Table 4. Figure 4 shows the desorption profiles for the masses of relevance. The heating rate, β, was 10 K min^{-1}. Four main temperature domains of desorption were observed, in comparison to unreduced CeO_2, the reduced nature of the CeO_2 surface has altered the product desorption profiles. The first desorption temperature for both ethanol and acetaldehyde shifted from 455 to 495 K. The second desorption temperature at 570 K is composed exclusively of acetaldehyde. Acetaldehyde remains as the major product with its relative yield increasing slightly. Acetone was observed again, desorbing at the slightly higher temperature of 690 K. Yield, however, increased to 0.018 of the carbon balance. Carbon monoxide and carbon dioxide desorbed at increased rates when the experiment reached conclusion (773 K), indicating much higher desorption temperatures. Yields were therefore determined by assuming that the peak was at 773 K and extrapolating a symmetric peak, from which the area could be deduced. There are several comparisons that can be drawn from the two TPD profiles presented above. First, the reduction of the metal oxide changes the behaviour of ethanol desorption on the surface of ceria. Acetaldehyde desorption at the high temperature domain on the reduced CeO_2 was more accentuated than on unreduced CeO_2. Second, the reduced catalyst containing Ce^{3+} cations (23) shows greater activity towards product formation with unreacted ethanol yield showing a 17% drop. Acetone, barely accountable on CeO_2, increases by a factor of 3 on the reduced catalyst. Third, with the exception of acetaldehyde all other species desorbed at a slightly higher peak temperature on the reduced CeO_2. This difference in peak temperature averages around 50 K.

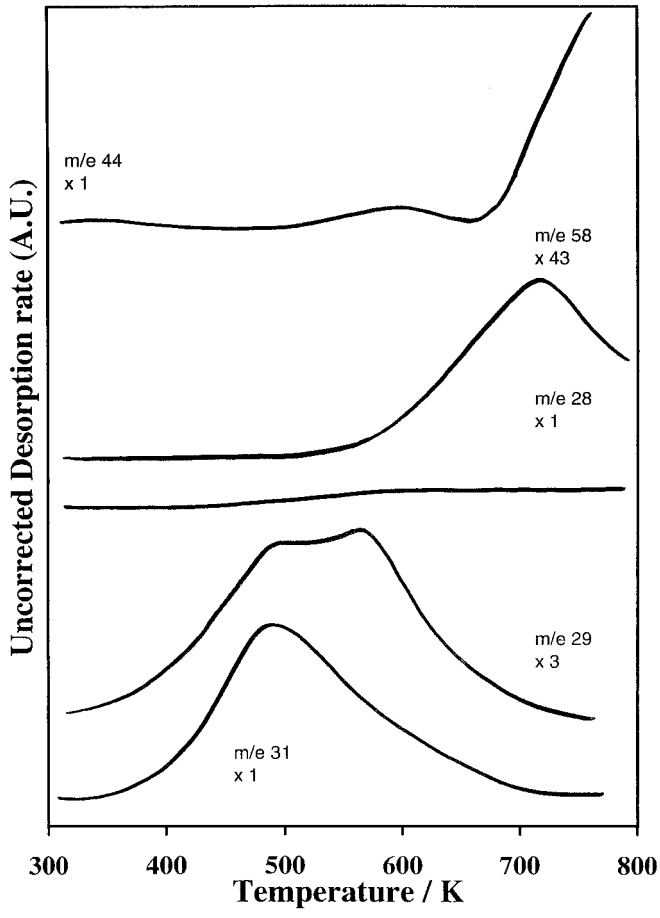

FIG. 4. Product desorption profiles from TPD after ethanol adsorption on H_2-reduced CeO_2 at room temperature.

TABLE 4

Product Analysis of Ethanol-TPD on H_2-Reduced CeO_2

Product	Peak temperature (K)	Yield	Carbon selectivity (%)
Acetone	690	0.018	5.9
Acetaldehyde	495, 570	0.114	37.7
Carbon dioxide	>750	0.060	19.9
Carbon monoxide	>750	0.043	14.4
Ethanol	495	0.698	—
Methane	730	0.066	21.9

Of interest is the fact that there is a tendency towards yields of products with masses less than the mass of the reactant, ethanol, with acetone an exception. Acetone desorption on unreduced CeO_2 results from acetate ketonisation. Acetates are formed upon partial oxidation of ethoxide species by surface oxygen anions. FT-IR data have shown that both ethoxides and acetates are readily observed on CeO_2 surfaces upon ethanol adsorption at room temperature (see FT-IR results below). This provides clear evidence that dissociation together with oxidation reactions dominate on the surface.

TABLE 5

Product Analysis of Ethanol-TPD on Unreduced Pd/CeO_2

Product	Peak temperature (K)	Yield	Carbon selectivity (%)
Acetone	495	0.003	0.4
Acetaldehyde	395	0.040	5.5
Benzene	580	0.030	4.0
Carbon dioxide	580	0.340	47.3
Carbon monoxide	580	0.290	40.4
Ethanol	465	0.290	—
Methane	550	0.017	2.4

TPD experiments with acetaldehyde (23) adsorbed on CeO_2 showed the production of crotonaldehyde ($m/e = 70$, 69). Crotonaldehyde is a product of β-aldolisation of acetaldehyde and was not visible in these experiments. The other obvious aldehyde, formaldehyde ($m/e = 29$, 30, 27), is also not present. Other products that were checked for, but not observed, included benzene, acetic acid, ethylene, ethane, crotyl alcohol, and diethyl ether. The absence of ethylene and diethyl ether is a clear indication that CeO_2 (both unreduced and reduced) favours dehydrogenation of primary alcohols (i.e., ethanol) to aldehydes (i.e., acetaldehyde) and not dehydration (to form ethylene and/or diethyl ether).

TPD after ethanol adsorption on 1 wt% Pd/CeO_2. Shown in Table 5 are the fractional product yields, along with the carbon selectivity, of Pd/CeO_2. Desorption profiles of masses are shown in Fig. 5. Carbon monoxide and carbon dioxide are by far the dominant reaction products on Pd/CeO_2, desorbing at the highest temperature domain of 580 K. Collectively these combustion products account for 63% of the total carbon budget. Benzene (C_6H_6, $m/e = 78$, 77) was formed and desorbed at the same temperature domain as the carbonates. Acetaldehyde (CH_3CHO, $m/e = 29$, 44, 43), the major organic product, desorbed at the low temperature domain of 395 K. Unreacted ethanol (CH_3CH_2OH, $m/e = 31$, 45, 29) is relatively low, accounting for 0.29 of the fractional yield and desorbing at 465 K. A small amount (0.003) of acetone (CH_3COCH_3, $m/e = 43$, 58, 15) was detected and desorbed at 495 K.

TPD after ethanol adsorption on H_2-reduced 1 wt% Pd/CeO_2. Table 6 presents the fractional yields and carbon selectivities from ethanol-TPD over H_2-reduced Pd/CeO_2. Desorption profiles are shown in Fig. 6. Both the product distribution and the desorption temperatures are similar to those of ethanol-TPD over unreduced Pd/CeO_2. Three differences are, however, noticed. First, benzene selectivity dramatically decreased from 5.5 (unreduced Pd/CeO_2) to 0.6% (reduced Pd/CeO_2); second, acetone desorption increased considerably, from 0.4 (unreduced Pd/CeO_2) to 7.9% (reduced Pd/CeO_2); third, acetaldehyde selectivity increased twofold on the reduced surface.

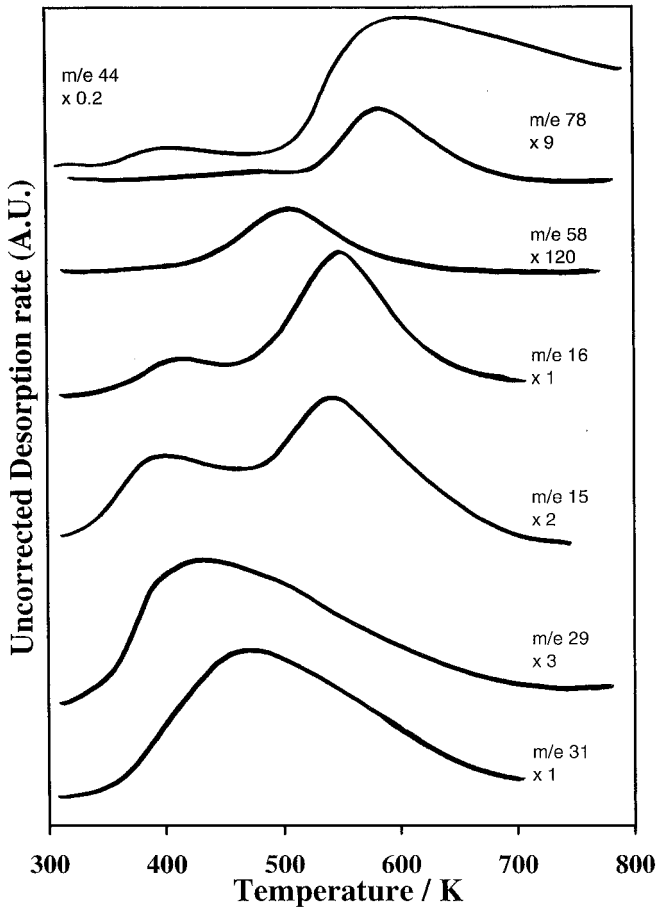

FIG. 5. Product desorption profiles from TPD after ethanol adsorption on 1 wt% Pd/CeO_2.

4. FT-IR Spectroscopy

Ethanol adsorption on unreduced CeO_2. The spectrum in Fig. 7a presents IR features at 2960, 2836, 2696, 1572, 1474, 1424, 1383, 1292, 1107, and 1057 cm^{-1} obtained after exposing CeO_2 to ethanol at 309 K. The bands at 2960,

TABLE 6

Product Analysis of Ethanol-TPD on H_2-Reduced Pd/CeO_2

Product	Peak temperature (K)	Yield	Carbon selectivity (%)
Acetone	580	0.050	7.9
Acetaldehyde	410	0.066	10.6
Benzene	610	0.003	0.6
Carbon dioxide	610	0.310	49.3
Carbon monoxide	610	0.165	26.3
Ethanol	410	0.370	—
Methane	570	0.031	5.1

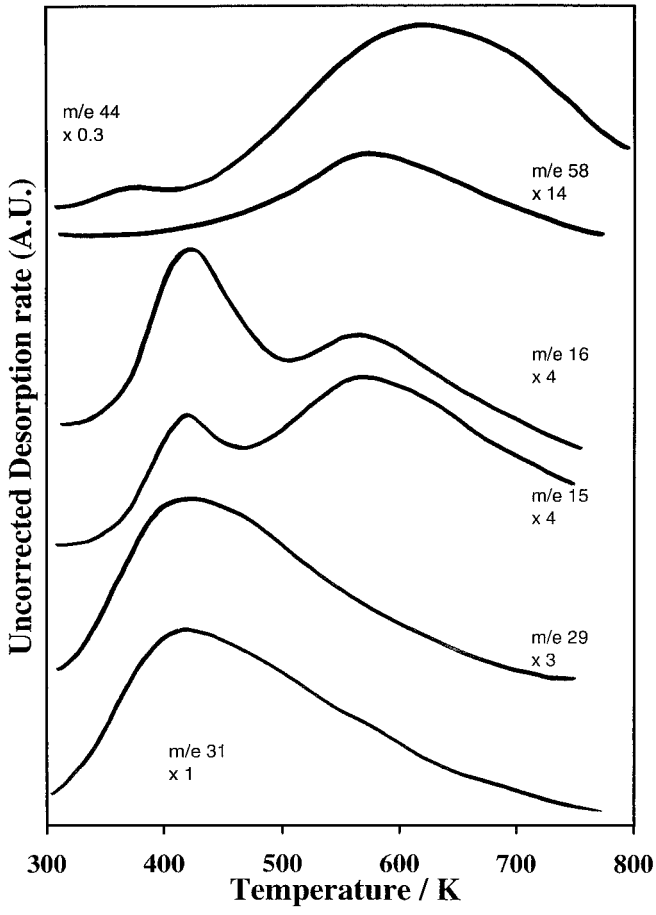

FIG. 6. Product desorption profiles from TPD after ethanol adsorption on H_2-reduced 1 wt% Pd/CeO_2.

2836, and 2696 $\nu(CH_3,CH_2)$, 1474 $\delta_{as}(CH_3, CH_2)$, 1383 $\delta_s(CH_3, CH_2)$, and 1107 and 1057 ν(C–O) cm^{-1} can be attributed to surface ethoxide species, with the band at 2696 cm^{-1} arising from fermi resonance of the C–H deformation band at 1474 cm^{-1}. Table 7 lists the assignments of the vibrational modes for adsorbed ethoxides and ethanol over CeO_2 and 1 wt% Pd/CeO_2 from this study and over various other surfaces. The formation of adsorbed surface ethoxide species was first spectroscopically reported by Greenler (42), who adsorbed ethanol on aluminium oxide at 308 K. Subsequently, surface ethoxide species have been identified on zinc oxide (43), magnesium oxide (44), Cu(100) (45), and Ni(111) (46a), among others. The assignment of the 1292 cm^{-1} ethoxide band is tentative; literature sources have attributed this band to the δ(OH) of molecular ethanol (27, 41), whilst Zhang *et al.* (37) have assigned it to a twisting mode of the C–H group of the ethoxide species upon ethanol adsorption on 1% MoO_3/SiO_2.

The two distinct bands at 1107 and 1057 cm^{-1} attributed to ν(C–O) indicate that two kinds of adsorbed ethoxide species are formed on CeO_2. They may be characterised as monodentate and bidentate species by the C–O stretches at 1107 and 1057 cm^{-1}, respectively. Multiple adsorbed alkoxide species have been observed on CeO_2; Li *et al.* (13) identified two kinds of methoxide species upon adsorption of methanol on CeO_2 at 300 K. Whilst three types of methoxide species, again from methanol adsorption on CeO_2, have been reported and attributed to monodentate, bidentate, and tridentate methoxide species (15, 16).

The band at 1572 cm^{-1} (flanked by shoulders at 1578 and 1553 cm^{-1}) is attributed to the ν_{as}(OCO) mode of acetate species while that at 1424 cm^{-1} is attributed to the ν_s(OCO) of the same species. The difference between the two bands, $\Delta\nu = 148$ cm^{-1}, tends towards a bidentate (chelating) configuration (46b). To confirm the assignment of acetate species, acetic acid was adsorbed on CeO_2 at 355 K (Fig. 7b). Bands at 1580 ν_{as}(OCO), 1429 ν_s(OCO), 1306 $\delta(CH_3)$, and 1026 $\rho(CH_3)$ cm^{-1} were observed, and are characteristic of acetate species. The formation of carboxylates, in particular

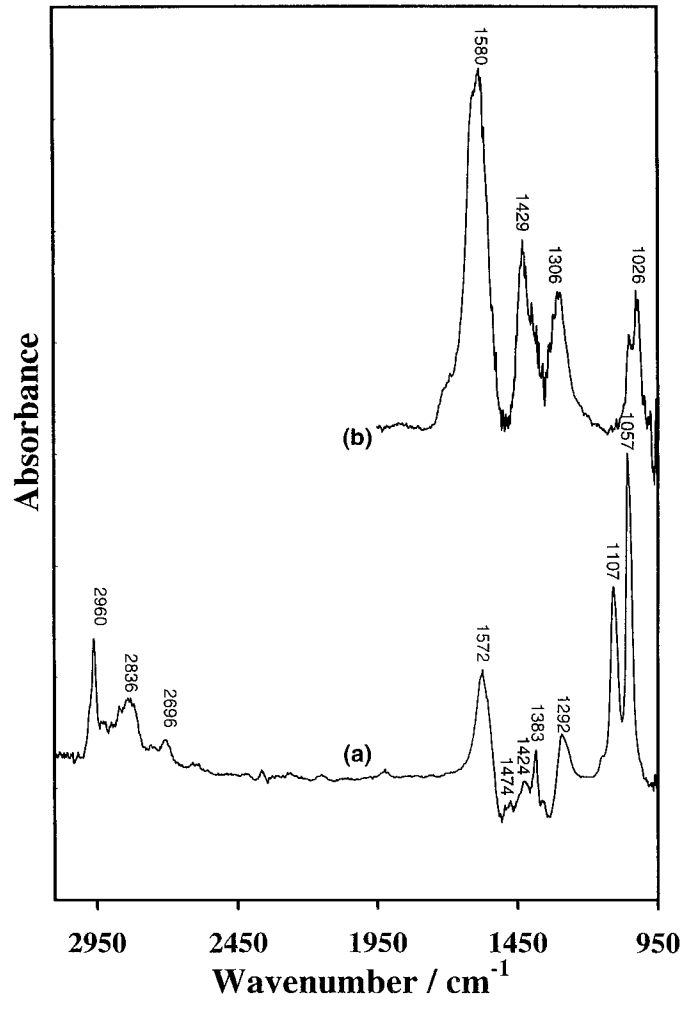

FIG. 7. FT-IR spectra of unreduced CeO_2 after adsorption of (a) ethanol and (b) acetic acid at 309 K.

TABLE 7

IR Vibrational Frequencies and Mode Assignments for Ethoxide Species from the Adsorption of Ethanol on CeO_2, Pd/CeO_2, and Various Catalysts

Mode	CeO_2 (this work)	γ-Al_2O_3 (40)	1% MoO_3/SiO_2[a] (37)	SiO_2 (41)	1 wt% Pd/CeO_2 (this work)	Pd(111) (27)
$\nu_{as}(CH_3)$	2960	2970	2972	2982	2982	2925
$\nu_{as}(CH_2)$	—	2930	—	—	2934	—
$\nu_s(CH_2)$	2836	2900	2872, 2892	—	2909	—
$\nu_s(CH_3)$	—	2870	2928	2932	2880	—
$\delta(CH_2)$	1473	—	—	1496, 1484	1478	1465
$\delta_{as}(CH_3)$	—	1450	—	1452	1451	—
$\delta_s(CH_3)$	1383	1390	—	1378	1397	1400
$\delta(CH_2)+\delta_{as}(CH_3)$	—	—	1446, 1452	—	—	—
$\tau(CH_2)$	—	—	1274, 1292	—	—	—
ν(C–O)	—	1170	—	—	—	—
ν(C–O)	1107	1115	—	—	1078	—
ν(C–O)	1057	1070	1030	—	1037	1040

[a] Values from laser Raman spectroscopy.

acetate species, have been observed on a number of oxides. Surface acetate species (1572 and 1466 cm^{-1}) have been observed upon heating ethanol-adsorbed aluminium oxide to 443 K (42). Kagel and Greenler (47) have also shown that methoxide species, from the adsorption of methanol on MgO, are capable of transforming into formate species upon heating to 438 K. Furthermore, Li *et al.* (13) observed the formation of formate species upon adsorption of formic acid on CeO_2, with bands at 2845 ν(C–H), 1599, 1553, and 1542 ν_{as}(OCO), 1362 and 1248 ν_s(OCO), and 1371 δ(C–H) cm^{-1}. Formate formation has also been observed on other oxides, including Al_2O_3 (42, 48), ZnO (49–51), TiO_2 (52), MoO_3 (53), ZrO_2 (54), and MgO (55).

Band assignments of acetate species, directly formed upon adsorption of acetic acid, have been reported on several oxides such as TiO_2 (21) and Fe_2O_3 (56). Table 8 shows the infrared bands observed on CeO_2 at 373 K together with data from literature on other oxides. Several bands in the 1000–1100 cm^{-1} region were observed, 1050, 1026, and 1019 cm^{-1}. Comparison with CH_3COONa (57) indicates that these bands are due to the rocking modes of CH_3 (ν_{10} and ν_{14}). The band at 1296 cm^{-1} may be attributed to $2\nu_5$, while the band at 1692 cm^{-1} is most likely due to ν_5 (ca. 645 cm^{-1}) + ν_{14} (1051 cm^{-1}). The other bands are as assigned in Table 8. In order to gain more information regarding acetate species over CeO_2, we have heated the dosed CeO_2 surface to several temperatures. Heating the surface to 423 K did not cause observable change of the infrared bands, and the ratio of the band intensity of the asymmetric OCO stretch (1580 cm^{-1}) to symmetric OCO stretch (1426 cm^{-1}) remained unchanged (ca. 2.1). Further heating to 573 K did not result in any dramatic change of the bands, although the band at ca. 1020 cm^{-1} increased slightly in intensity. Heating the oxide to 673 K considerably attenuated the bands in the 1000–1100 cm^{-1} region, while the band at 1580 cm^{-1} was shifted slightly to 1574 cm^{-1} and the ν_s(OCO) band remained unchanged; the difference between the two bands exhibits a bidentate type. The absorbance of all bands decreased slightly at this temperature. No evidence of aldehyde or ethoxide species were observed at all the investigated temperatures.

Evidence of transformation of bidentate acetate species to carbonate species is given upon heating the surface. The band at 1578 cm^{-1} decreases in intensity while a new band is formed at 1568 cm^{-1} (Fig. 8A, (c) to (f)). The band at 1568 cm^{-1} together with that at 1341 cm^{-1} is similar to other literature bands attributed to bidentate carbonates (such as those at 1580, 1320 cm^{-1}, TiO_2 (anatase); 1560, 1340 cm^{-1}, αCr_2O_3; 1565, 1310 cm^{-1}, La_2O_3 (60a)). The intense band at 1420 cm^{-1} observed at 623 K (Fig. 8B, (e)) and above is

TABLE 8

IR Vibrational Frequencies and Mode Assignments for Adsorbed Acetate Species from the Adsorption of Acetic Acid on CeO_2 and Various Oxides, Including CH_3COONa and CH_3COOK

Mode	TiO_2 (21)	ZnO (55)	α-Fe_2O_3 (56)	CeO_2 (this work)	CH_3COONa (57)	CH_3COOK (57)
$\nu_{as}(CH_3)$	3018	—	—	2970	2989	3010
$\nu_s(CH_3)$	2939	2940	—	2933	2936	2935
ν_{as}(OCO)	1587	1554	1540	1580	1578	1556
						1693
$\delta_{as}(CH_3)$	1459	1460	—	1437	1443	1429
	1672				1498	1456
ν_s(OCO)	—	1427	1427	1426	1414	1413
$\delta_s(CH_3)$	1421	1311	—	1304	1340	1344
$\rho(CH_3)$	1334	—	—	1051	1052	—
				1026	1020	
				1019		

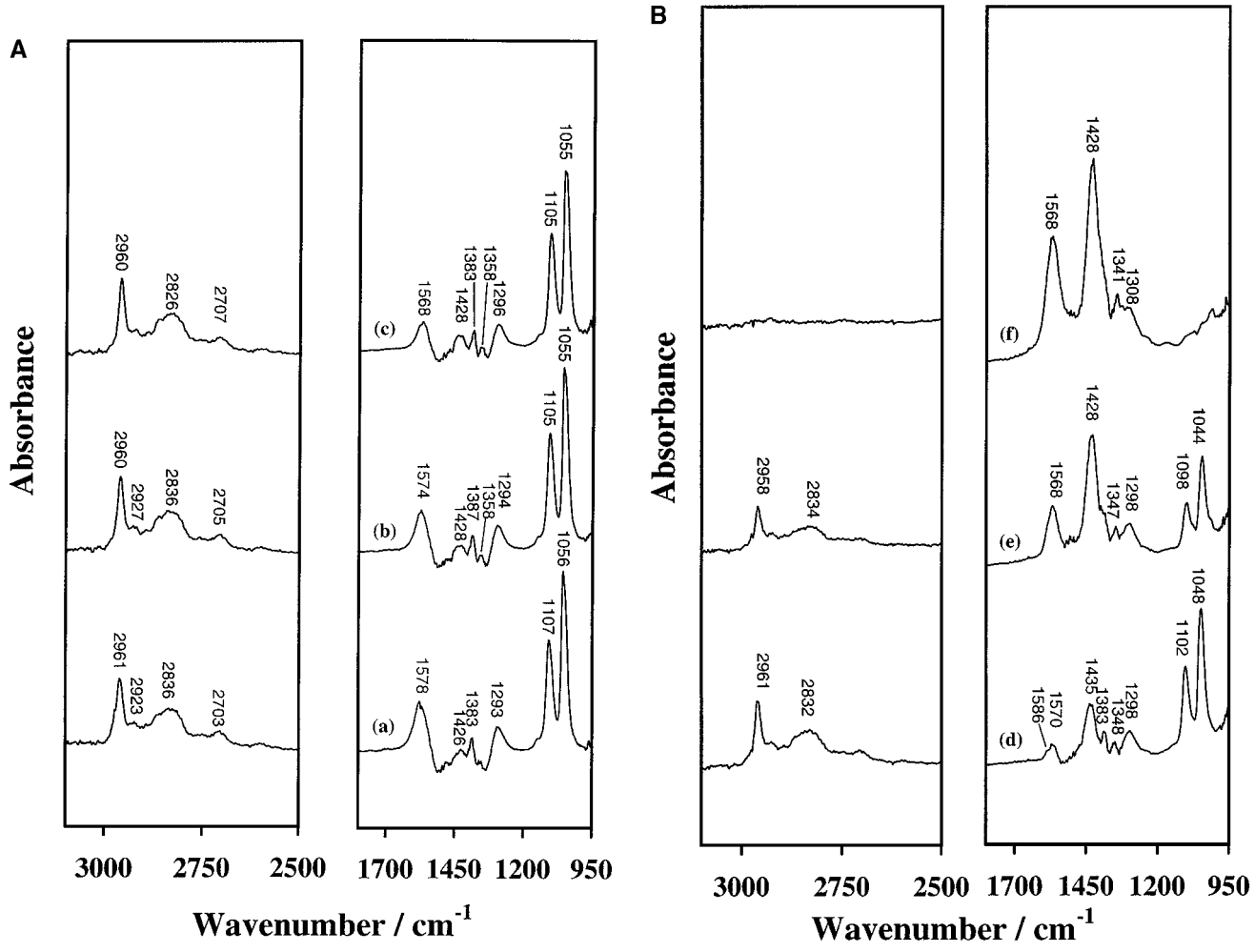

FIG. 8. (A) FT-IR spectra after adsorption of ethanol (1.50 Torr, 3 min, evacuation at 6×10^{-5} Torr) at 309 K on unreduced CeO_2 and subsequent heating to (a) 373, (b) 423, and (c) 473 K. All spectra recorded at 309 K. (B) FT-IR spectra after adsorption of ethanol (1.50 Torr, 3 min, evacuation at 6×10^{-5} Torr) at 309 K on unreduced CeO_2 and subsequent heating to (d) 573, (e) 623, and (f) 673 K. All spectra recorded at 309 K.

not due to the ν_s(OCO) of acetates, since the corresponding ν_{as}(OCO) has disappeared. This band is attributed to symmetric carbonate species (60a).

Figure 9 presents the uncorrected band intensities corresponding to species adsorbed on CeO_2 as a function of temperature. An initial slight increase in the intensity of ethoxide bands is noticed; this is most likely due to the effect of heating the reactor cell, which may have caused readsorption of unreacted ethanol outgassed from the reactor walls on the CeO_2 surface. Overall there is a decrease in intensity of the bands attributed to ethoxide (1057 and 1107 cm^{-1}) and acetate (1572 cm^{-1}) species. The formation of carbonates (1568, 1428, and 1341 cm^{-1}) from further oxidation of acetate species is detected at 423 K. Carbonates are the dominating species at higher temperatures. At 673 K, no peaks attributed to either ethoxides or acetates are observed.

Ethanol adsorption on H_2-reduced CeO_2. The adsorption of ethanol on H_2-reduced CeO_2 at room temperature produced bands at 2963 ν(CH), 1449 $\delta(CH_3, CH_2)$, 1385 $\delta(CH_3, CH_2)$, 1104 ν(C–O), and 1058 ν(C–O) cm^{-1}, which are readily assigned to adsorbed surface ethoxide species (Fig. 10). As seen previously on the unreduced CeO_2 surface, two types of ethoxide species were formed and are characterised by the two ν(C–O) bands at 1105 and 1058 cm^{-1} as monodentate and bidentate species, respectively. These bands progressively decreased in intensity from 423 to 573 K, disappearing completely at 623 K (Fig. 10).

H_2-reduced CeO_2 displayed no evidence of acetate formation upon ethanol adsorption at this temperature, indicating that the reduced CeO_2 surface does not possess sufficient oxygen atoms for acetate formation. A weak band at 1541 cm^{-1} was detected when the catalyst was

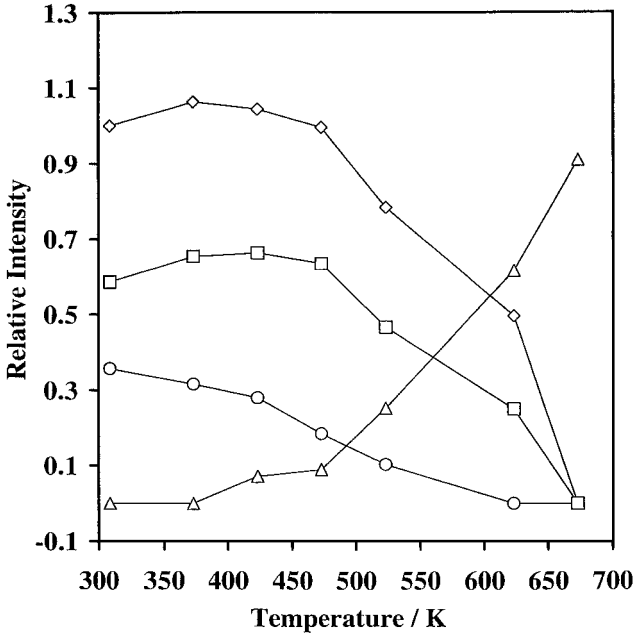

FIG. 9. Uncorrected relative band intensities of the (◇) 1057 and (□) 1107 cm^{-1} ethoxide, (○) 1572 cm^{-1} acetate, and (△) 1427 cm^{-1} carbonate species on unreduced CeO_2 as a function of temperature.

heated to 423 K; further heating broadened this band and at 523 K it developed into a sharp feature, with a shoulder at 1553 cm^{-1}. The band at 1541 cm^{-1} is attributed to a bidentate carbonate species, whilst the shoulder at 1553 cm^{-1} is assigned to acetate species. Two other bands situated at 1438 and 1343 cm^{-1} were also apparent at 523 K and, together with the band at 1541 cm^{-1}, increased in intensity with temperature. These new bands are assigned to the stretching modes of carbonate species. At 673 K the only remaining species on the surface were those associated with carbonates, the 1541 and 1343 cm^{-1} bands shifting in wavenumber to 1538 and 1345 cm^{-1}, respectively, whilst the band at 1438 cm^{-1} remained unchanged. No bands related to adsorbed acetaldehyde have been observed during ethanol-FT-IR experiments on both CeO_2 and H_2-reduced CeO_2 surfaces.

Ethanol adsorption on 1 wt% Pd/CeO₂. Figure 11 shows the spectrum of 1 wt% Pd/CeO_2 after adsorption of ethanol at room temperature. Bands corresponding to adsorbed ethoxide species were observed at 2982 $\nu_{as}(CH_3)$, 2934 $\nu_{as}(CH_2)$, 2909 $\nu_s(CH_2)$, 2880 $\nu_{as}(CH_3)$, 1478 $\delta(CH_2)$, 1451 $\delta_{as}(CH_3)$, 1397 $\delta_{as}(CH_3)$, 1343 $\delta(CH_3, CH_2)$, 1078 ν(C–O), and 1037 ν(C–O) cm^{-1}. These bands progressively decreased in intensity upon heating and were not detected at 523 K and above. On Pd/CeO_2, predominantly one ν_{as}(C–O) band was observed at 1037 cm^{-1}, suggesting that adsorption of ethanol on Pd/CeO_2 resulted primarily in one form of ethoxide species. In contrast to ethanol adsorption on unreduced CeO_2, bands corresponding to acetate species were not observed at room temperature. However, at 473 K a moderate band at 1519 cm^{-1} was detected and may be ascribed to adsorbed carbonate species. The intensity of this band increased markedly upon heating, with a shift to lower wavenumbers.

A band at 1711 cm^{-1} was observed at 373 K and increased considerably in intensity upon heating to 473 K. The development of this band coincided with the appearance of a weak band at 1125 cm^{-1}. At 523 K, both features declined in intensity dramatically, with the 1125 cm^{-1} band no longer distinguishable. The bands at 1711 and 1125 cm^{-1} are attributed to the ν(C=O) and ν(C–O), ν(C–C) of an acetaldehyde species, respectively. Additional bands located at 1659, 1637, and 1171 cm^{-1} were also observed at 473 K, and they declined upon heating to 523 K with the appearance of a weak band at 1601 cm^{-1}. These bands were not detected at higher temperatures. The bands at 1659, 1637, and 1171 cm^{-1} may be assigned to the ν(C–O), ν(C=C) and $\rho(CH_3)$, ν(C–C) of a crotonaldehyde species. These assignments are in good agreement with spectra obtained

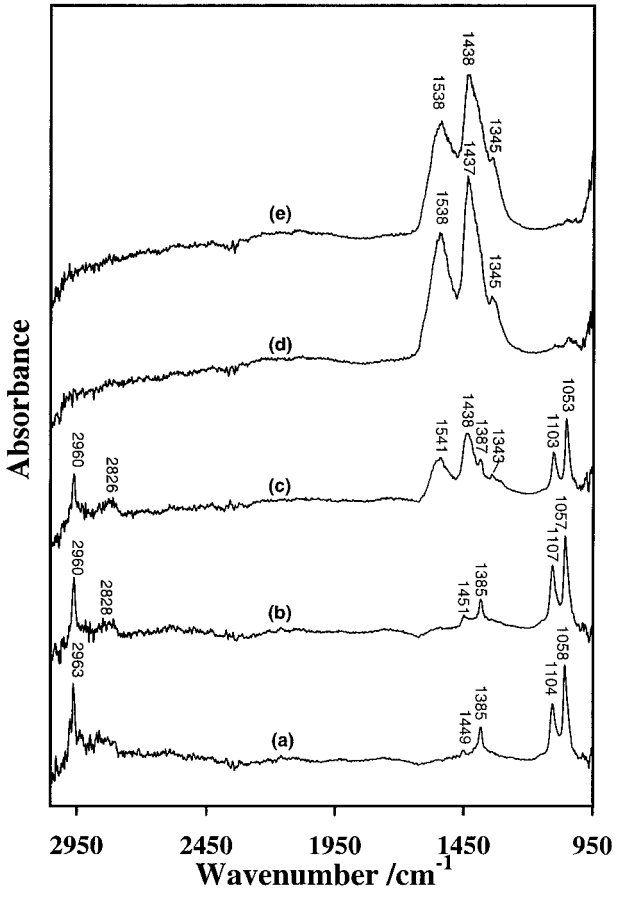

FIG. 10. FT-IR spectra after adsorption of ethanol (1.50 Torr, 3 min, evacuation at 6×10^{-5} Torr) on H_2-reduced CeO_2 at (a) 309 K and subsequent heating to (b) 423, (c) 523, (d) 623, and (e) 673 K. All spectra recorded at 309 K.

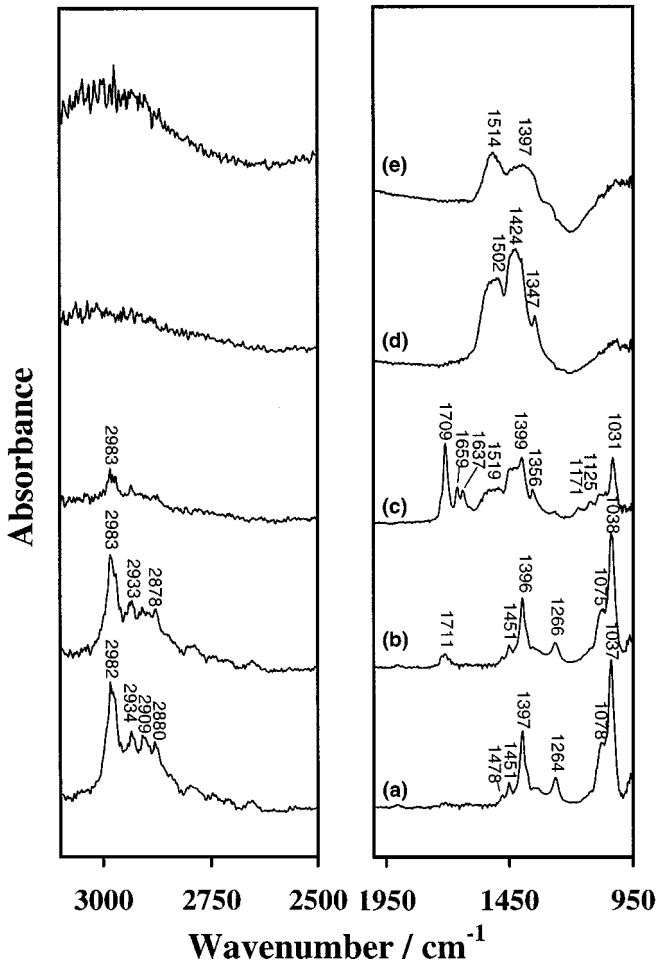

FIG. 11. FT-IR spectra after the adsorption of ethanol at (a) 309 K on unreduced 1 wt% Pd/CeO_2 and subsequent heating to (b) 373, (c) 473, (d) 575, and (e) 673 K. All spectra recorded at 309 K.

from the adsorption of crotonaldehyde on 1 wt% Pd/CeO_2 (spectrum not shown) at room temperature, in which bands at 1651, ν(C=O), 1634, ν(C=C), 1445, δ(CH), 1395, δ(CH), and 1160, ν(CC), $\rho(CH_3)$ cm^{-1} were observed. The 1601 cm^{-1} band may correspond to the $\delta(H_2O)$ mode; water is a byproduct from the adolisation reaction that forms crotonaldehyde and is discussed in the following section. A broad band situated at ca. 2133 cm^{-1} was detected at 473 K, the intensity of this band increased slightly upon heating to 523 K but was diminished at higher temperatures. The band at ca. 2134 cm^{-1} is attributed to adsorbed carbon monoxide. In addition, features corresponding to the formation of monodentate carbonate species were also detected at 473 K. These bands shifted to 1517, 1433, and 1347 cm^{-1} and increased in intensity upon heating to 573 K. However, further heating to 737 K decreased these bands slightly.

Ethanol adsorption on H_2-reduced 1 wt% Pd/CeO_2. The effect of reduction temperature in relation to metal-support interaction was investigated by performing the reduction at two temperatures, low temperature reduction (LTR) at 550 K and high temperature reduction (HTR) at 755 K. The spectrum (Fig. 12) of LTR-Pd/CeO_2 after adsorption of ethanol at 309 K resembles that of unreduced Pd/CeO_2. Bands corresponding to ethoxide species were observed at 2983 $\nu_{as}(CH_3)$, 2934 $\nu_{as}(CH_2)$, 2911 $\nu_s(CH_2)$, 2880 $\nu_s(CH_3)$, 1477 (CH_2), 1453 $\delta_{as}(CH_3)$, 1397 $\delta_s(CH_3)$, 1086 ν(C–O), and 1039 ν(C–O) cm^{-1}. Heating to higher temperatures effectively decreased the intensity of these features until, by 523 K, they were no longer detected.

An acetaldehyde species, characterised by weak bands at 1704 (ν(C=O)) and 1148 ν(C–O), ν(C–C) cm^{-1}, were detected at 423 K. Upon heating to 473 K, a slight increase in the intensity of the 1704 cm^{-1} band and additional bands at 1534, 1449, and 1352 cm^{-1} were observed. The 1704 and 1148 cm^{-1} bands were not detected at 523 K. An increase of the additional three bands was observed with a corresponding shift to 1527, 1442, 1349 cm^{-1}. The bands at 1527, 1442, and 1349 cm^{-1} are attributed to monodentate carbonate species. The bands at 1534 and 1352 cm^{-1}, which were observed at 473 K, may be attributed to carboxylate species.

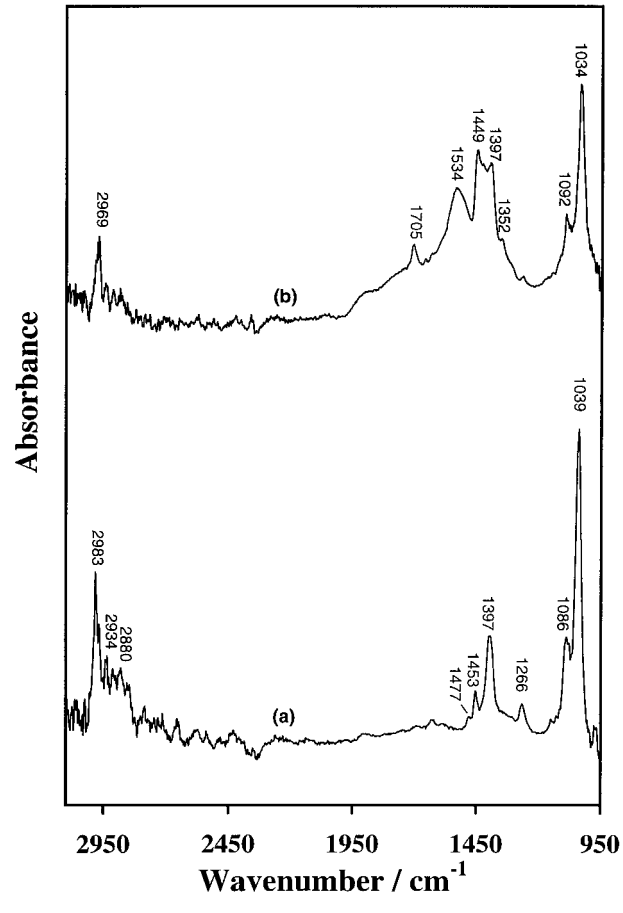

FIG. 12. FT-IR spectra after adsorption of ethanol on LTR-Pd/CeO_2 at (a) 309 and (b) 473 K. All spectra recorded at 309 K.

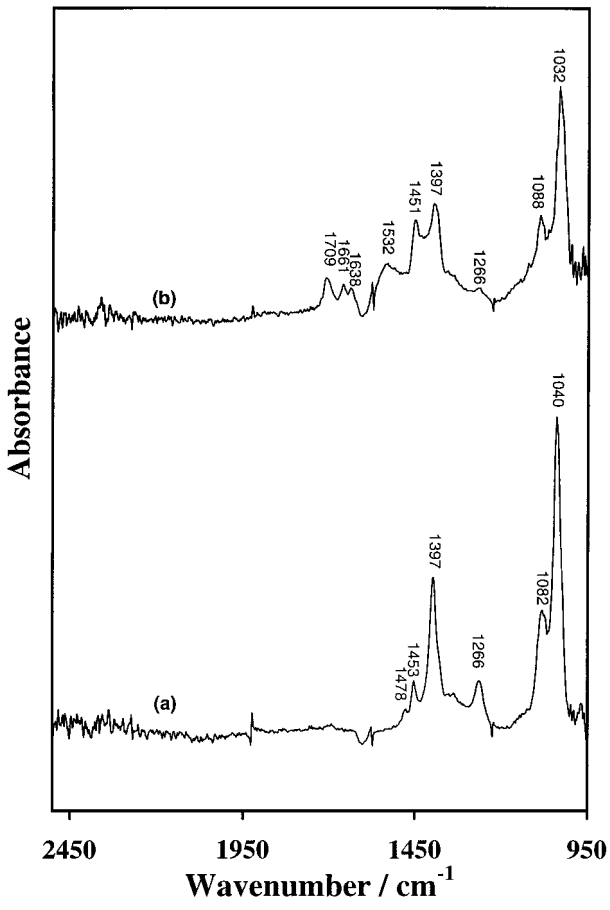

FIG. 13. FT-IR spectra after adsorption of ethanol on HTR-Pd/CeO_2 at (a) 309 and (b) 473 K. All spectra recorded at 309 K.

Figure 13 shows the spectrum of HTR-Pd/CeO_2 after the adsorption of ethanol at 309 K. The region beyond 2500 cm^{-1} is not well resolved because of noise as a consequence of the extent of reduction. Again, bands corresponding to surface ethoxide species (1478 $\delta(CH_3)$, 1453 $\delta_{as}(CH_3)$, 1397 $\delta_s(CH_3)$, 1082 ν(C–O), and 1040 ν(C–O) cm^{-1}) were observed, which upon heating were effectively decreased, with complete decomposition by 573 K. At 423 K, a weak band at 1705 cm^{-1} was detected, and heating to 473 K increased the intensity of this band. Furthermore, four additional bands at 1661, 1638, 1146, and 1121 cm^{-1} were also detected at 473 K. Similar bands were also observed on unreduced Pd/CeO_2. The band at 1705 cm^{-1}, together with those at 1611, 1637, 1146, and 1121 cm^{-1}, disappeared upon heating to higher temperatures. The bands at 1705 (ν(C=O)) and 1121 (ν(C–O), ν(C–C)) cm^{-1} are attributed to an acetaldehyde species, whilst those at 1661, 1637, and 1146 are assigned to crotonaldehyde. The appearance of bands at 1532 and 1451 cm^{-1} were also detected at 473 K. Heating to higher temperatures ($\geq$573 K) increased the intensity of these bands, and the band at 1532 cm^{-1} was down-shifted to 1526 cm^{-1} along with the development of a band at 1347 cm^{-1}. The features at 1526 and 1347 cm^{-1} are attributed to bidentate carbonate species, while that at 1347 cm^{-1} is attributed to symmetric carbonate ions.

DISCUSSION

The results of ethanol reactions over CeO_2, H_2-reduced CeO_2, Pd/CeO_2, and H_2-reduced Pd/CeO_2 may be summarised as follows.

(1) Steady state reactions show (i) a zero reaction order dependency for diatomic oxygen at and above ca. 20%, and (ii) addition of Pd to CeO_2 decreased the apparent activation energy of reaction by 35.5 kJ mol^{-1} and increased the rate constant by almost one order of magnitude.

(2) TPD data indicates that (i) while acetaldehyde desorbed in two temperature domains on CeO_2 (at 455 and 585 K), it desorbed as one peak on H_2-reduced CeO_2 (555 K), as well as on Pd/CeO_2 (395 K) and H_2-reduced Pd/CeO_2 (410 K), (ii) ethanol conversion to other products was as follows, 15% (CeO_2), 30.2% (H_2-reduced CeO_2), 71% (Pd/CeO_2), and 63% (H_2-reduced Pd/CeO_2), (iii) while acetone was observed on all surfaces, the desorption temperatures were considerably lower on Pd/CeO_2 than on CeO_2, suggesting a different reaction pathway, and (iv) benzene formation was only observed on Pd/CeO_2 catalysts and H_2-reduction decreased its formation to almost negligible amounts.

(3) FT-IR results show that (i) acetate species were only detected on unreduced CeO_2 surfaces at room temperature, on all the other surfaces higher temperatures were required to oxidise ethoxide species (observed on the four surfaces) to acetates, (ii) no evidence of adsorbed CO (resulting from C–C bond dissociation) is observed at all temperatures (up to ca. 700 K) on CeO_2 and below 473 K on Pd/CeO_2, (iii) η^1-adsorbed acetaldehyde was observed on Pd/CeO_2 and H_2-reduced Pd/CeO_2 (no evidence of adsorbed acetaldehyde species is observed on CeO_2 surfaces), and (iv) adsorbed crotonaldehyde species on Pd/CeO_2 were observed.

In view of the above results one may divide the observed reactions on the surfaces of CeO_2 and Pd/CeO_2 into oxidation to acetates and ultimately to CO_2 via carbonates and hydrogenocarbonates (at temperatures >ca. 600 K), dehydrogenation to acetaldehyde, and carbon–carbon bond formation to acetone, crotonaldehyde, and benzene. Dehydrogenation and dehydration reactions of primary and secondary alcohols are one of the most commonly observed reactions on oxide materials (58–60b). Several factors may contribute to the dehydration versus dehydrogenation pathways of a particular reactant. These include (a) the metal-to-oxygen bond strength (large E_{M-O} orienting towards dehydration, small E_{M-O} orienting towards dehydrogenation (61, 62)), (b) surface structure affecting the coordination environment of cations (the presence of

double vacancies of a particular cation may accommodate two alkoxides that may then undergo a dehydration reaction to form ethers (63), and (c) oxygen electronic polarisability (64). Ethanol reactions on CeO_2 and Pd/CeO_2 resulted in the formation of acetaldehyde with no evidence of ethylene nor diethylether, in other words, no dehydration reactions. Since the work is conducted on polycrystalline material, it is less feasible to extract structural information. However, thermodynamic properties may be extracted. The bulk E_{M-O} may be computed by the formula (from Ref. (62))

$$y\Delta H_{M-O}(\text{ionic}) = -\Delta H_f(M_xO_y) + \Delta H_{sub}(M) + (y/2)\Delta H_{dis}(O_2) - y\sum EA(O) + x\sum IE(M), \quad [1]$$

where

$\Delta H_f(M_xO_y)$ is heat of formation
$\Delta H_{sub}(M)$ is heat of sublimation of the metal
$\Delta H_{dis}(O_2)$ is dissociation energy of diatomic oxygen
$\sum EA(O)$ is sum of the first and second electron affinities for oxygen, and
$\sum IE(M)$ is sum of the first through $2y/x$ ionisation energies.

In this calculation the heats of sublimation were taken from Ref. (65), and the heats of formation, dissociation energy of diatomic oxygen, electron affinities of oxygen, and ionization energies of $M = Ce$ were taken from Ref. (66). The strength of the metal–oxygen bond of the bulk oxide was estimated by dividing $y\Delta H_{M-O}$ by the coordination number of oxygen in cerium oxide, $C_O, = 4$. For simplicity $y\Delta H_{M-O}/C_o$ is substituted by E_{M-O}, which is equal to 2,200 kJ mol^{-1} of oxygen for CeO_2. This is close to the E_{M-O} of TiO_2 (2,000 kJ mol^{-1}), both oxides catalyse the oxidative dehydrogenation of ethanol to acetaldehyde, and smaller than that of SiO_2 ($E_{M-O} = 3{,}300$), which is relatively unreactive (64).

The electronic polarisability may be computed following the Lorentz–Lorenz relationship (also known as the Clausius–Mossotti equation) (67),

$$\alpha = (3V_m/4\pi N_a)\cdot(\varepsilon-1)/(\varepsilon+2) \quad \text{or} \quad = (3V_m/4\pi N_a)\cdot(n^2-1)/(n^2+2), \quad \text{since } \varepsilon = n^2, \quad [2]$$

where V_m denotes molar volume, N_a Avogadro's number, ε the dielectric constant, and n the refractive index. The oxygen electronic polarisability, α_O, may be calculated from $\alpha_O = \frac{1}{z}(\alpha - a\alpha_{M^{z+}})$ for an oxide of the form M_aO_z, where $\alpha_{M^{z+}}$ is the polarisability of the cation. In a previous work (64) a relationship was observed between the rate constant of ethanol reaction and an empirical formula computed as

$$\ln k = 4.25\alpha - 14.84, \quad [3]$$

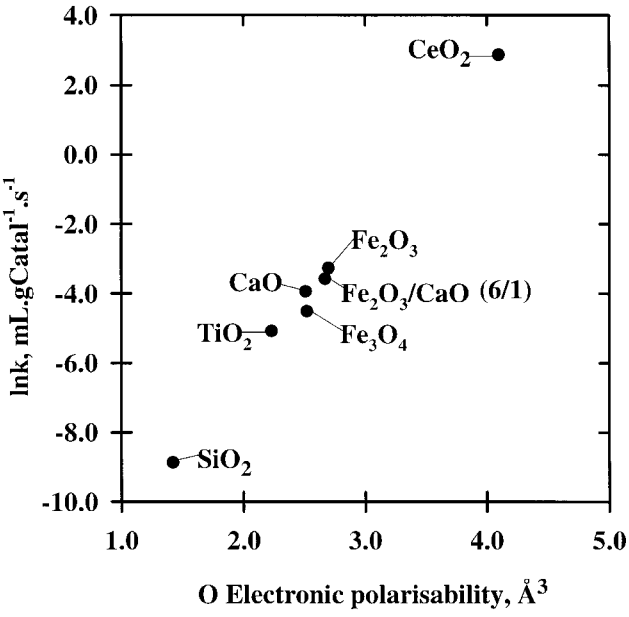

FIG. 14. Plot of ln(k) as a function of O electronic polarisibility for a series of oxides, CeO_2 from this work, all other oxides from Ref. (64).

The experimental $\ln k_{473\,K}$ for CeO_2 is 2.8 mL g^{-1} s^{-1}. Figure 14 shows this relationship (data for the other oxides are from Ref. (64)).

Carboxylate formation upon aldehyde adsorption has been observed on several oxides such as ZnO (68), MgO (69), CeO_2 (23), and TiO_2 (70). The driving force for this reaction is oxygen donation from the surface to the adsorbate. Upon ethanol adsorption on the surface and the formation of ethoxides (Table 7), acetates are the only additional species observed. This indicates that dehydrogenation to acetaldehyde is followed by a very facile oxidation making acetates as

$$CH_3CH_2OH + Ce^{+4}\text{-}O^{-2} \rightarrow CH_3CH_2OCe^{+4} + OH(a) \quad [4]$$

$$CH_3CH_2OCe^{+4} \rightarrow CH_3CHOCe^{+4} + H(a) \quad [5]$$

$$CH_3CHOCe^{+4} + O^{-2} \rightarrow CH_3COOCe^{+4} + H(a). \quad [6]$$

Table 8 presents the band assignment of acetate species observed on CeO_2 (this work) together with those of acetate species on other oxides. The absence of acetate species on the H_2-reduced CeO_2 (in flow, as indicated in the experimental part) is explained by surface depletion of the mobile oxygen (surface defects). It is important to mention that batch reduction of CeO_2 with H_2 (1.5 Torr at 750 K for 2×30 min, vacuum evacuation (ca. 5×10^{-5} torr) in between) did decrease but not eliminate acetate species formation from ethanol. This, in fact, is consistent with the thermodynamic property of CeO_2/Ce_2O_3, where at 700 K $p(H_2O)p(H_2)^{-1} = 9.6 \times 10^{-7}$ (78). Thus, water buildup during reduction in batch is sufficient to back-oxidise Ce_2O_3

to CeO_2. The absence of acetate species on Pd/CeO_2 can be explained in view of XPS data (Table 1) that indicates important decrease of the O to Ce atomic ratio. We have investigated the effect of addition of other noble metals (Pt and Rh) to CeO_2 on the XPS O(1*s*)/Ce($3d_{5/2,3/2}$) ratios and found that they do also decrease this ratio when compared to CeO_2 alone; the XPS O(1*s*)/Ce($3d_{5/2,3/2}$) were 1.91 and 1.59 for Rh/CeO_2 and Pt/CeO_2 respectively (79). Thus, the addition of Pd, Pt, or Rh to CeO_2 resulted in partial reduction of CeO_2 surfaces, which is evidenced by the absence of carboxylates in the IR spectra. The presence of η^1-adsorbed acetaldehyde species on Pd/CeO_2 is most likely due to two factors, the high yield of this surface to acetaldehyde (steady state kinetics shows that the rate constant is about one order of magnitude on Pd/CeO_2 when compared to CeO_2, and TPD results indicate a fourteenfold increase) and the surface oxygen depletion which inhibits the oxidation route.

Several products containing higher carbon number than ethanol are observed. These are acetone, crotonaldehyde, and benzene. The desorption of acetone was at two distinct temperatures, high temperature desorption on unreduced CeO_2 (630 K) and H_2-reduced CeO_2 (690 K) and low temperature desorption on unreduced Pd/CeO_2 (495 K) and H_2-reduced Pd/CeO_2 (580 K). The shift in desorption temperatures of more than 100 K in both cases (unreduced and reduced) is most likely due to a different reaction mechanism. On CeO_2 where acetate species are evident even at room temperature, acetone formation is due to coupling of two acetates as

$$2\,CH_3COOCe^{+4} \rightarrow CH_3COCH_3 + CO_2 + Ce^{+4}\text{-}O^{-2} + Ce^{+x}\text{-}V_O, \quad [7]$$

where V_O denotes oxygen vacancy and $x < 4$.

On the other hand, acetone formation on Pd/CeO_2 may be explained by a disproportionation reaction of two acetyl species (formed from acetaldehyde) to give one molecule of acetone and one molecule of CO as

$$2\,CH_3CHO \rightarrow 2\,H(a) + 2\,CH_3CO(a) \quad [8]$$

$$2\,CH_3CO(a) \rightarrow CH_3COCH_3 + CO. \quad [9]$$

This latter reaction has been previously studied on Pd/CeO_2 and Pd-Co/CeO_2 (from acetaldehyde) (23).

Evidence of an adsorbed crotonaldehyde species has been given by IR (Fig. 11). Crotonaldehyde is the result of β-aldolisation of acetaldehyde on the surface of CeO_2. Aldolisation of acetaldehyde was previously observed on other surfaces, including CeO_2 (23), TiO_2 (25), and Cu/Zn/Al (30). It requires, in addition to Lewis acid sites at which to bind two molecules of acetaldehyde, a base site to abstract a hydrogen atom from the α position of the carbonyl.

The efficient production of benzene in a homogeneously catalysed reaction is well known for transition metal compounds (71). In particular, the Reppe synthesis of cyclooctatetraene by the tetramerisation of acetylene using a mononuclear nickel catalyst can be made, by the addition of a phenylphosphine ligand, to produce the major byproduct (benzene) exclusively (72). This involves the arrangement of the acetylene molecules in close proximity, the "template" effect. Heterogeneously catalysed aromatisation reactions are less common and yet, for the production of benzene, toluene, and xylene, still receive considerable attention (73). Molybdenum, in particular, has proved itself very effective at producing benzene on a variety of supports (SiO_2 and ZSM-5 zeolite) with high selectivity (60–90%) (74). The reaction mechanism of benzene formation from acetylene has been studied (75–77). Acetylene adsorbs in the three-hollow site on Pd(111) and distorts so that the carbon atoms are approximately sp^2 hybridised with the C–C axis parallel to the metal surface. This reacts with a C_4H_4 metallocycle via a Diels–Alder cycloaddition reaction resulting in benzene formation (77). The combination of IR and TPD data, in this work, suggests the following. (1) The absence of ethylene and acetylene in the desorption profile may indicate that C–O bond dissociation of a species precursor to an adsorbed acetylene is the limiting step. (2) IR analysis has shown no evidence of adsorbed benzene species or other adsorbed hydrocarbons. (3) However, IR shows two intense bands at 1659 and 1638 cm^{-1} that are attributed to an adsorbed crotonaldehyde species. (4) These species might be converted to a C_4H_4 species that reacts with a C_2H_x species giving benzene. H_2-reduction results in the almost disappearance of benzene during TPD. Although, it may in a first reasoning appear contradictory to the overall scheme of benzene formation from C_2—oxygen predosing of Pd(111) surfaces results in inhibition of C_6H_6 formation—there is, in fact, a reasonable explanation. The H_2-reduction of the oxide surface inhibits the β-aldolisation route (due to a considerable decrease of the Lewis-base sites, oxygen anions) thus inhibition of this reaction pathway occurs.

CONCLUSIONS

The reaction of ethanol has been studied on unreduced and H_2-reduced CeO_2 and Pd/CeO_2 by TPD, IR, and steady state kinetics. At room temperature acetate species were only observed on unreduced CeO_2. The reaction rate constant of ethanol on CeO_2 fitted very well with a previously proposed relationship between the oxygen polarisability of the oxide and the rate constant. In spite of the one order of magnitude increase in the dehydrogenation reaction yield of ethanol to acetaldehyde in presence of Pd, no evidence of acetate species was observed. This latter result combined with XPS data (as well as with a similar work over Pt/CeO_2 and Rh/CeO_2 (79)) indicates that Pd addition to CeO_2 resulted in considerable reduction of the oxide support.

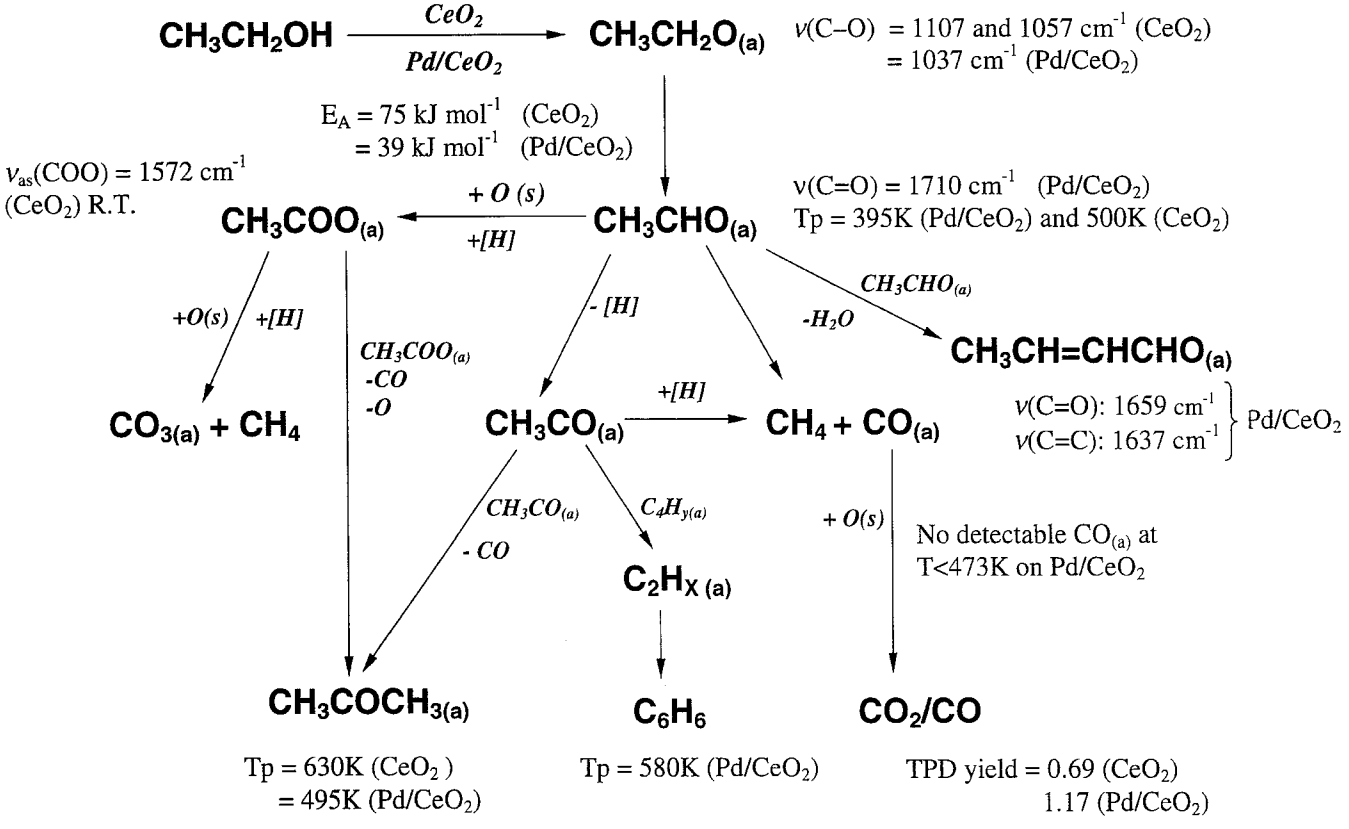

SCHEME 1. Reaction pathways of ethanol over CeO_2 and Pd/CeO_2.

Besides acetaldehyde, acetone and benzene were also observed by TPD. Acetone is most likely synthesised via two different reaction mechanisms, one on the oxide (acetate coupling) and another in presence of Pd (acetyl disproportionation). The absence of ethylene, acetylene, and butadiene during TPD and the presence of IR bands assigned to crotonaldehyde suggests that benzene formation may be formed through a C_2H_x species (from ethoxides) + C_4H_y species (from crotonaldehyde). The Scheme 1 summarises the reaction pathways observed during this work.

REFERENCES

1. Gandhi, H. S., Piken, A. G., Shelef, M., and Delosh, R. G., SAE Paper 760201, 1976.
2. Su, E. C., Montreuil, C. N., and Rothchild, W. G., *Appl. Catal.* **17**, 75 (1985).
3. Harrison, B., Diwell, A. F., and Hallett, C., *Platinum Met. Rev.* **32**, 73 (1988).
4. Kim, G., *Ind. Eng. Chem. Prod. Res. Dev.* **21**, 267 (1982).
5. Hoflund, G. B., Gardner, S. D., Schryer, D. R., Upchurch, B. T., and Kielin, E. J., *React. Kinet. Catal. Lett.* **58**, 19 (1996).
6. Sergeys, F. J., Masellei, J. M., and Ernest, M. V., W. R. Grace Co., U.S. Patent 3,903,020, 1974.
7. Hinden, S. G., Engelhard Mineral and Chemical Co., U.S. Patent 3,870,455, 1973.
8. Yao, H. C., and Yao, Y. F., *J. Catal.* **86**, 254 (1984).
9. Bernal, S., Botana, F., Calvino, J., Cauqui, M., Cifredo, G., Jobacho, A., Pintado, J., and Rodriguez-Izquierdo, J., *J. Phys. Chem.* **97**, 4118 (1993).
10. Perrichon, V., Laachir, A., Bergeret, G., Fréty, R., Tournayan, L., and Touret, O., *J. Chem. Soc. Faraday Trans.* **90**, 773 (1994).
11. Fierro, J., Soria, J., Sanz, J., and Rojo, J., *J. Solid State Chem.* **66**, 154 (1987).
12. *Design News*, June 22, p. 86 (1998).
13. Li, C., Domen, K., Maruya, K., and Onishi, T., *J. Catal.* **125**, 445 (1990).
14. Demri, D., Chateau, L., Hindermann, J. P., Kiennemann, A., and Bettahar, M. M., *J. Molec. Catal. A Chem.* **104**, 237 (1996).
15. Badri, A., Binet, C., and Lavalley, J. C., *J. Chem. Soc. Faraday Trans.* **93**, 1159 (1997).
16. Lamotte, J., Morávek, V., Bensitel, M., and Lavalley, J. C., *React. Kinet. Catal. Lett.* **36**, 113 (1988).
17. Henrich, V. E., and Cox, P. A., "The Surface Science of Metal Oxides." Cambridge Univ. Press, Cambridge, USA, 1994.
18. Vohs, J. M., and Barteau, M. A., *Surf. Sci.* **176**, 91 (1986).
19. Chauvin, C., Vallet, A., Lavalley, J. C., Idriss, H., Hindermann, J. P., Kiennemann, A., and Chaumette, P., *J. Catal.* **121**, 56 (1990).
20. Raskó, J., Bontovics, J., and Solymosi, F., *J. Catal.* **146**, 22 (1994).
21. Boaventura, J., Ph.D. dissertation, University of Delaware, 1989.
22. Madix, R. J., *Adv. Catal.* **29**, 1 (1982).
23. Idriss, H., Diagne, C., Hindermann, J. P., Kiennemann, A., and Barteau, M. A., *J. Catal.* **155**, 219 (1995).
24. Davis, J. L., and Barteau, M. A., *Surf. Sci.* **256**, 50 (1991).
25. Idriss, H., Kim, K. S., and Barteau, M. A., *J. Catal.* **139**, 119 (1993).
26. Madhavaram, H., and Idriss, H., in preparation, 1998.
27. Davis, J. L., and Barteau, M. A., *Surf. Sci.* **235**, 235 (1990).

28. Shekhar, R., Barteau, M. A., Plank, R. V., and Vohs, J. M., *J. Phys. Chem.* **101**, 7939 (1997).
29. Boujana, S., Demri, D., Cressely, J., Kiennemann, A., and Hindermann, J. P., *Catal. Lett.* **7**, 359 (1990).
30. Kiennemann, A., Idriss, H., Kieffer, R., Chaumette, P., and Durand, D., *Ind. Eng. Chem. Res. Dev.* **30**, 1130 (1991).
31. McCabe, R. W., and Mitchell, P. J., *Ind. Eng. Chem. Res. Dev.* **23**, 196 (1984).
32. Idriss, H., Libby, M., and Barteau, M. A., *Catal. Lett.* **15**, 13 (1992).
33. Barr, T. L., Fries, C. G., Cariti, F., Bart, J. C. J., and Giordano, N., *J. Chem. Soc. Dalton Trans.*, 1825 (1983).
34. Kim, K. S., Gossman, A. F., and Winograd, N., *Anal. Chem.* **46**, 197 (1974).
35. Ko, E. I., Benziger, J. B., and Madix, R. J., *J. Catal.* **62**, 264 (1980).
36. Idriss, H., Kim, K. S., and Barteau, M. A., *J. Catal.* **139**, 119 (1993).
37. Zhang, W., Desikan, A., and Oyama, S. T., *J. Phys. Chem.* **99**, 14468 (1995).
38. Doca, N., and Segal, E., *Rev. Roumaine Chim.* **31**, 567 (1986).
39. Tu, Y. J., Li, C., and Chen, Y. W., *J. Chem. Tech. Biotechnol.* **59**, 141 (1994).
40. Golay, S., Doepper, R., and Renken, A., *Appl. Catal. A Gen.* **172**, 97 (1998).
41. Natal-Santiago, M. A., and Dumesic, J. A., *J. Catal.* **175**, 252 (1998).
42. Greenler, R. G., *J. Chem. Phys.* **37**, 2094 (1962).
43. Nagao, M., and Morimoto, T., *J. Phys. Chem.* **84**, 2054 (1984).
44. Aika, K., and Lunsford, J. H., *J. Phys. Chem.* **81**, 1393 (1977).
45. Camplin, J. P., and McCash, E. M., *Surf. Sci.* **360**, 229 (1996).
46. (a) Gates, S. M., Russell, J. N., and Yates, J. T., *Surf. Sci.* **171**, 111 (1986); (b) Deacon, G. B., and Phillips, R. J., *Coordin. Chem. Rev.* **33**, 227 (1980). [and references therein]
47. Kagel, R. O., and Greenler, R. G., *J. Chem. Phys.* **49**, 1638 (1968).
48. Lamotte, J., Saur, O., and Lavalley, J. C., *J. Chem. Soc. Faraday Trans. I* **82**, 3019 (1986).
49. Ahkter, S., Cheng, W. H., Lui, K., and Kung, H. H., *J. Catal.* **85**, 437 (1984).
50. Ahkter, S., Lui, K., and Kung, H. H., *J. Phys. Chem.* **89**, 1958 (1985).
51. Bowker, M., Houghton, H., and Waugh, K. C., *J. Chem. Soc. Faraday Trans. I* **77**, 3023 (1981).
52. Hattori, H., and Wang, G., *in* "Proceedings, 8th International Congress On Catalysis, Berlin, 1984," Vol. II. Dechema, Frankfurt-am-Maim, 1984.
53. Chung, J. S., Miranda, P., and Bennett, C. O., *J. Chem. Soc. Faraday Trans. I* **86**, 19 (1985).
54. Abe, H., Maruya, K., Domen, K., and Onishi, T., *Chem. Lett.*, 1875 (1984).
55. Spitz, R. N., Barton, J. E., Barteau, M. A., Staley, R. H., and Sleight, A. W., *J. Phys. Chem.* **90**, 4067 (1986).
56. Lorenzelli, V., Busca, G., and Sheppard, N., *J. Catal.* **66**, 28 (1980).
57. Ito, K., and Bernstein, H. J., *Can. J. Chem.* **34**, 170 (1956).
58. Matsumura, Y., Hashimoto, K., and Yoshida, S., *J. Chem. Soc. Chem. Commun.*, 1599 (1987).
59. Halasz, I., Vinek, H., Thomke, K., and Noller, H., *Z. Phys. Chem.* **163**, 157 (1985).
60. (a) Busca, G., and Lorenzelli, V., *Mat. Chem.* **7**, 89 (1982) [and references therein]; (b) McKenze, A., Fishel, C., and Davis, R., *J. Catal.* **138**, 547 (1992).
61. Rethwisch, D. G., and Dumesic, J. A., *Appl. Catal.* **21**, 97 (1986).
62. Rethwisch, D. G., and Dumesic, J. A., *Langmuir* **2**, 73 (1986).
63. Kim, K. S., and Barteau, M. A., *Surf. Sci.* **223**, 13 (1989).
64. Idriss, H., and Seebauer, E. G., submitted, 1999.
65. Katz, J. J., Seaborg, G. T., and Morss, L. R., "The Chemistry of the Actinide Elements," Vol. 2, 2nd ed., p. 1281. Chapman & Hall, New York, 1986.
66. Lide, D. R., Ed.-in-Chief, "Handbook of Chemistry and Physics," 76th ed., 1995–1996.
67. Duffy, J. A., "Bonding, Energy Levels and Bands in Inorganic Solids." Longman Scientific and Technical/Wiley, Glasgow, 1990.
68. Vohs, J. M., and Barteau, M. A., *Langmuir* **5**, 965 (1989).
69. Peng, M. C., and Barteau, M. A., *Langmuir* **5**, 1051 (1989).
70. Rekoske, J. E., and Barteau, M. A., *Langmuir*, in press.
71. "Organometallic Mechanism and Catalysis." Academic Press, New York, 1978.
72. Schauzer, G. N., and Eichlwer, S., *Chem. Ber.* **95**, 550 (1962).
73. Wang, D. J., Lunsford, J. H., and Rosynek, M. P., *Catal. Lett.* **3**, 289 (1996).
74. Germain, J. E., "Catalytic Conversion of Hydrocarbons." Academic Press, London, 1969.
75. Patterson, C. H., and Lambert, R. M., *J. Phys. Chem.* **92**, 1266 (1988).
76. Ramirezcuesta, A., Zgrablich, G., and Tysoe, W. T., *Surf. Sci.* **340**, 109 (1995).
77. Ormerod, R. M., Lambert, R. M., Hoffman, H., Zaera, F., Yao, J. M., Saldin, D. K., Wang, L. P., Bennet, D. W., and Tysoe, W. T., *Surf. Sci.* **295**, 277 (1993).
78. Barin, I., "Thermochemical Data of Pure Substances, Part 1," 2nd ed. VCH, New York, 1993.
79. Yee, A., Morrison, S. J., and Idriss, H., *in* "16th North American Meeting of the Catalysis Society, Boston, MA," June 1999.